



**HAL**  
open science

## Performance of a monofiber optical probe in determining the droplet size and velocity in spray systems comparing with a high-speed camera

Kritchart Wongwailikhit, Nicolas Dietrich, Gilles Hébrard, Pisut Painmanakul

### ► To cite this version:

Kritchart Wongwailikhit, Nicolas Dietrich, Gilles Hébrard, Pisut Painmanakul. Performance of a monofiber optical probe in determining the droplet size and velocity in spray systems comparing with a high-speed camera. Industrial and engineering chemistry research, 2019, 10.1021/acs.iecr.9b02446 . hal-02350501

**HAL Id: hal-02350501**

**<https://hal.insa-toulouse.fr/hal-02350501>**

Submitted on 23 Jun 2021

**HAL** is a multi-disciplinary open access archive for the deposit and dissemination of scientific research documents, whether they are published or not. The documents may come from teaching and research institutions in France or abroad, or from public or private research centers.

L'archive ouverte pluridisciplinaire **HAL**, est destinée au dépôt et à la diffusion de documents scientifiques de niveau recherche, publiés ou non, émanant des établissements d'enseignement et de recherche français ou étrangers, des laboratoires publics ou privés.

# PERFORMANCE OF A MONOFIBER OPTICAL PROBE IN DETERMINING THE DROPLET SIZE AND VELOCITY IN SPRAY SYSTEMS COMPARING WITH A HIGH-SPEED CAMERA

Kritchart Wongwailikhit<sup>1,2</sup>, Nicolas Dietrich<sup>2</sup> and Gilles Hébrard<sup>2</sup>, Pisut Painmanakul<sup>1,3,a</sup>

<sup>1</sup> Department of Environmental Engineering, Faculty of Engineering, Chulalongkorn University, Bangkok, Thailand 10330

<sup>2</sup> LISBP, Université de Toulouse, INSA, INRA, CNRS, Toulouse, France

<sup>3</sup> Center of Excellence on Hazardous Substance Management (HSM), Chulalongkorn University, Thailand

Corresponding author: <sup>a</sup>pisut.p@chula.ac.th

## Abstract

The ability of a monofiber optical probe to characterize the hydrodynamics in spray systems was compared with that of a high-speed camera. Initially, the performance of both techniques was determined on the same droplets by using a syringe to produce a series of droplets. The optical probe gave a discrepancy according to the high-speed camera mainly due to the fact that the image processing of the high-speed camera photos determined the velocity from the movement of the droplet centroid while the optical probe determined the interfacial velocity from its collision with a droplet. The droplet oscillation occurred since the droplet formation process and droplet coalescence on the probe eventually led to the discrepancy. However, when comparing both techniques statistically, their results were not apparently different. Secondly, a full-cone industrial nozzle was used to provide the spray. The average velocities from the two characterization techniques were then in close agreement; the oscillation and coalescence effects became insignificant due to less dense, the smaller sizes and the higher velocities of the droplets. However, the collision on the probe tip was off center and the difference in size limits still caused the discrepancy, especially for the size distribution. Nevertheless, a major advantage of the optical probe is that it is capable to determine the droplet hydrodynamics in dense spray conditions and enable the direct determination of the local liquid fraction, one of the important characteristics of a spray system.

## Keywords

optical probe, high-speed camera, spray, droplet size, droplet velocity

## 1. Introduction

Gas absorption using spray columns is now a frequently applied process in various applications, including the removal of volatile organic compounds (VOCs), hydrogen sulfide ( $H_2S$ ), nitrogen oxide ( $NO_x$ ), sulfur dioxide ( $SO_2$ ), and carbon dioxide ( $CO_2$ ) from contaminated gases (Bashipour et al., 2015; Raghunath and Mondal, 2016; Tamhankar et al., 2015; Tatin et al., 2015). In spray systems, the hydrodynamics of droplets play an important role in controlling the absorption efficiency of the sprays because the droplet sizes and velocities directly affect the interfacial area available for absorption (Roustan, 2003). If a spray system is to be understood and utilized efficiently, droplet size and velocity distributions need to be characterized (Hariz et al., 2017; Tatin et al., 2015). Various studies have proposed their mechanisms of droplet formation, including droplet sizes and velocities (Jones and Watkins, 2012; Nicholas P. Chermisinoff, 1986) and have been further used for the purposes of simulation, optimization, and design of the processes (Bandyopadhyay and Biswas, 2007; Darake et al., 2016). So far, the optical techniques of phase-doppler anemometry (PDA), droplet tracking velocimetry (DTV), or high-speed cameras have been successfully used to determine droplet sizes and velocities (Chigier, 1983; Husted et al., 2009; Tuck et al., 1997). However, most of the optical techniques encounter difficulties when used with dense spray or in conditions of poor visibility (Husted et al., 2009); Only a few techniques showed promising results, an optical flow estimation, for instance (Bung and Valero, 2016).

One of the techniques that can overcome such limitations is the phase detection probe. It was first pioneered by (Neal and Bankoff, 1963) as a technique for measuring multiphase flow characteristics. Since then, the probe has been widely used for the characterization of both gas phase dispersed in a liquid phase and liquid dispersed in a gas phase (Cartellier and Achard, 1991). Various works utilized the phase detection probes to determine the hydrodynamic of the air-water system, especially for high-velocity free surface flow (Felder and Chanson, 2015; Felder and Pfister, 2017; Zhang and Chanson, 2018) where the promising results were obtained. However, these probes have rarely been used in spray systems since responding to small, high-velocity droplets in such conditions requires an extremely high acquisition rate. Nevertheless, the optical probes have now overcome the difficulty. Various types of the optical probes have been considered for observing droplet hydrodynamics and the most suitable type for using in spray systems has been found to be the monofiber probe as its small size extends its ability to detect small droplets (Hong et al., 2004; Saito, 2017). The principle of the probe for determining the droplet hydrodynamics is based on the refractive index of the phase where the probe is located (Abuaf et al., 1978); different light intensity is sent back to a detector when the probe is exposed to different phases. Therefore, when a droplet collides with the probe, the detected light intensity changes due to the change in the phase covering the probe. Consequently, the droplet velocity and size can be determined from the change of the light intensity over the time that the droplet spends on the probe.

A major advantage of the probe is that it not only delivers velocity and size distributions but can also be used to directly determine the dispersed phase characteristics of sprays, such as a liquid fraction or droplet density. Various authors have utilized this advantage for the determination of the liquid fraction in their works (Stevenin et al., 2016a, 2016b) and most of the utilizations of optical probes on sprays nowadays concern only the liquid fraction. Although the methodology exists, few works have used the technique to measure droplet sizes or velocities (Marty et al., 2013; Valero and Bung, 2017), especially in cases of gas absorption; the optical probe is rarely used to determine the droplet hydrodynamics in actual spray conditions.

The objective of the work presented here is to fill this gap by identifying the performance of the optical probe in an actual spray system, compared with that of a high-speed camera in order to verify the probe performance and methodology visually. In the first section, a series of droplets using a syringe as a nozzle was investigated. The objective of this part is to compare the accuracy of the two techniques when the same droplets are observed. Afterward, a comparison experiment will be conducted in a spray system using an industrial nozzle. The probe limits, including the maximum velocity it can measure, the smallest size of droplet it can detect as well as droplet frequency approaching the probe, are analyzed and discussed.

## 2. Material and methods

### 2.1 Experimental setup

The purpose of the work was to determine the accuracy of an optical probe in spray conditions by comparing its results with those of a high-speed camera. However, when an industrial nozzle was used, it was difficult to identify the exact same droplets in both techniques. Therefore, the first part of the experiment used a syringe to produce a series of droplets that could be identified with certainty by both the optical probe and the high-speed camera. In the second part, an industrial nozzle was used to produce a commonly employed spray regime. For this part, the comparison was based on statistical approaches, giving average size and velocity, for instance.

#### 2.1.1 Acquisition of a droplet series

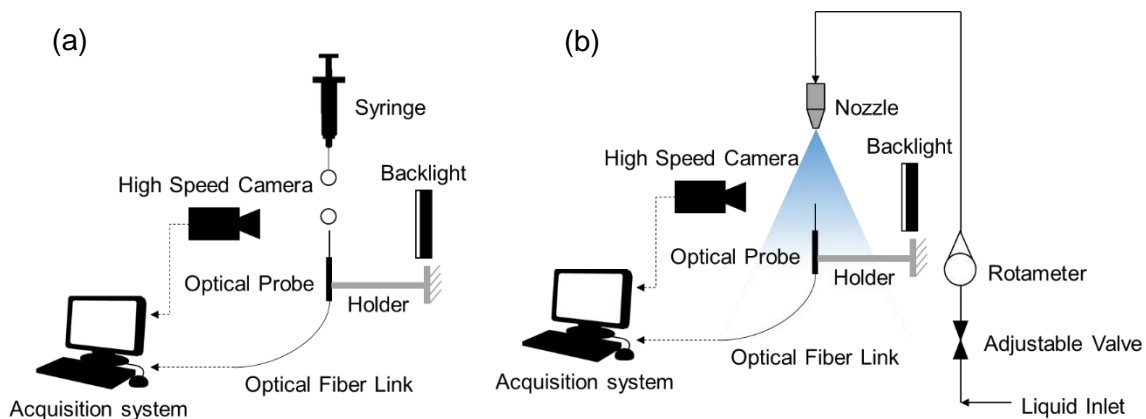


**Fig. 1** Experimental setup for  
(a) acquisition of a droplet series (b) acquisition of a spray condition

The experiment was set up as shown in Fig. 1(a). A syringe with a 0.5 mm tip size was positioned 5 mm above a monofiber optical probe (A2 Photonic Sensors, France). The syringe was filled with tap water and it could produce droplet sizes between 0.5 and 2.0 mm at a flow rate of 0.128 mL/s. After the injections, the droplet series produced with the syringe settled and came into contact with the optical probe. The signal from the probe was sent to the data acquisition system and analyzed by its software. A high-speed camera (Vision Research, Miro – M110, USA) was also set up to capture the trajectories of droplets, including their contacts with the optical probe. The signal from the optical probe and the photos of each droplet as it traveled were then analyzed to determine its size and velocity. The results from the two techniques were compared to assess the probe accuracy.

#### 2.1.2 Acquisition of a spray condition

The experimental setup is schematically depicted in Fig. 1(b). The water was fed through a spray nozzle at a flow rate that could be adjusted using the valve and rotameter. The optical probe and the high-speed camera were set up under the injection zone. Both camera and optical sensor were situated 5 cm below the nozzle. The distance between the camera and the center line of the nozzle was 20 cm. In this experiment, a 0.89 mm, full-cone spray nozzle QGA-SS1 from Spraying System Co. (USA) was used. The liquid flow rate was controlled at 0.59 L/min. Note that, in this experiment, many thousands of droplets were measured to ensure statistical accuracy of the results.

## 2.2 Image acquisition and treatment methodology

### 2.2.1 Image acquisition

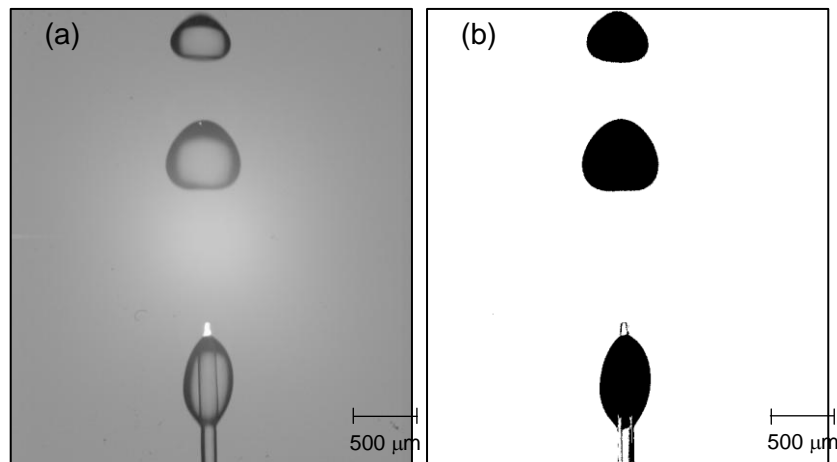


**Fig. 2** (a) Image captured with the camera and (b) Image processed with ImageJ for the same droplet observation

A high-speed camera from Vision Research, Phantom Miro – M110, was used for image acquisition. A backlight from PHLOX with a luminance of 30,383 cd/m<sup>2</sup> and uniformity of 93.65 % was set up as the image background. The photos were captured by National Optical, 704-155 DIN 4x Objective Lens at a framerate of 2,900 fps for the acquisition described in section 2.1.1 and by Carl Zeiss 50mm f/1.4 Planar at 32,000 fps and for the second part (industrial spray). An example of an image captured for the same droplets is shown in Fig. 2(a) for the same droplet observation and Fig. 3 for spray. The images were captured in an 8-bit grayscale format.

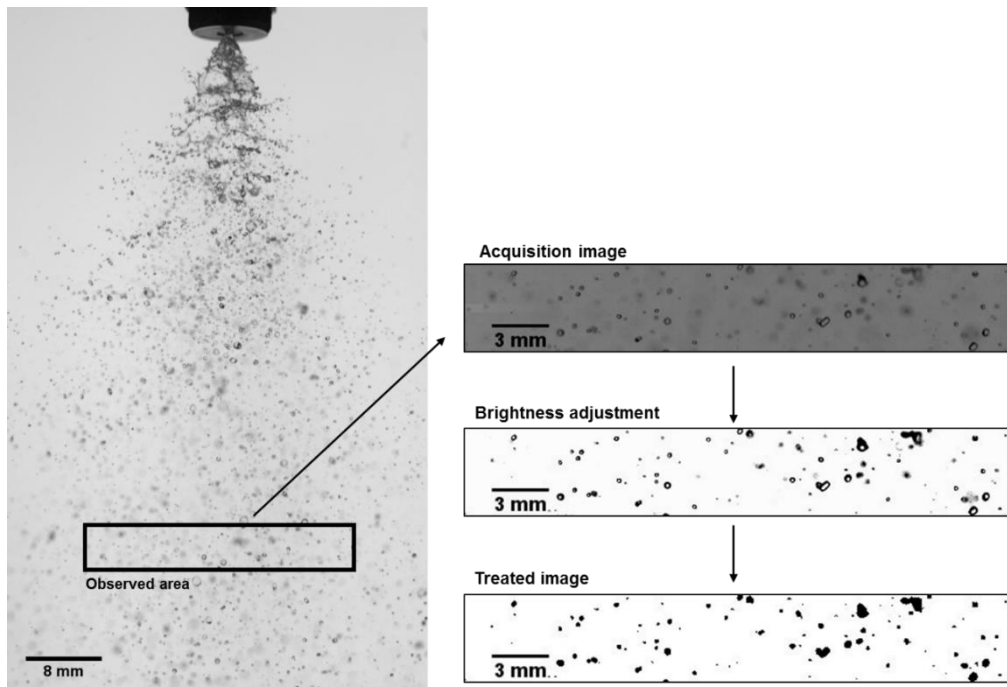


**Fig. 3** Image captured of a spray with 0.89 mm nozzle size when operating at 0.59 LPM and treated image

### 2.2.2 Determination of droplet size and velocity

To determine droplet velocity, the “wrtrack” plugin of ImageJ was used. This plugin tracked each droplet settling in the subsequent images. With the framerate used when capturing the images in the spray system with the industrial nozzle, droplet velocities of up to 25 m/s could be detected. However, the camera could detect only droplets larger than 0.1 mm because of the resolution limits of the camera and its lens.

### 2.2.3 Determination of droplet size

The captured images were processed and analyzed with ImageJ software. The most suitable level of gray (threshold) for each image was selected and the images were then converted into binary images as shown in Fig. 2(b) and Fig. 3 for the same droplet observation and a spray, respectively. These binary images were used to determine properties including the projected area (A) and perimeter (P). In this work, the equivalent spherical diameter for each droplet was used with the assumption that the projected shape of any droplet could be treated as an ellipse. This equivalent diameter could be determined with the correlation of (Heyt and Diaz, 1975) as shown in Equation (1), where  $d_e$  is the equivalent spherical diameter.

$$d_e = 1.55 A^{0.625} / P^{0.25} \quad (1)$$

## 2.3 Optical probe

### 2.3.1 Signal acquisition of a droplet

A monofiber optical probe from A2 Photonic Sensors (France) was used in this work. The probe was set up so as to be exposed to the spraying system and connected to its module. The minimum and maximum voltages were adjusted to -8 and +8 V, respectively.

The probe measured the maximum voltage value ( $V_G$ ) when it was exposed to air, and the minimum value ( $V_L$ ) when covered by water.

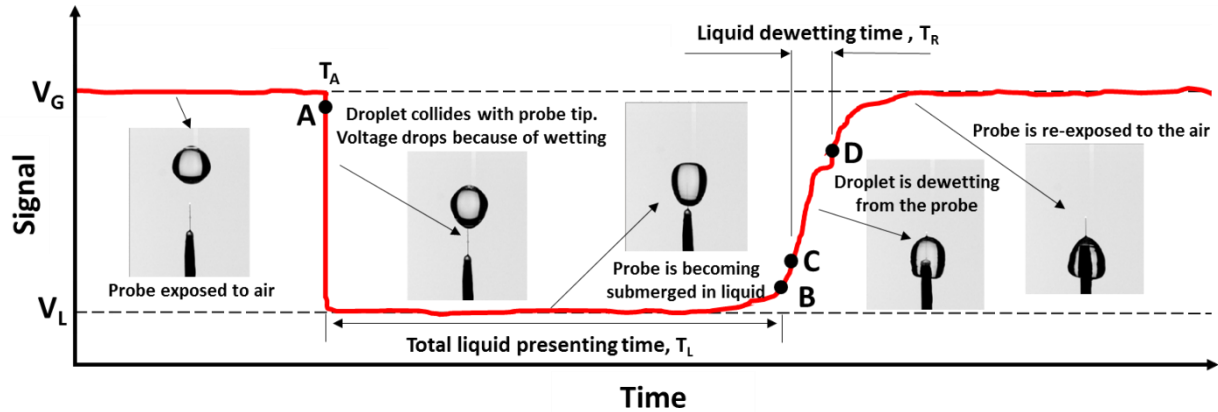


**Fig. 4** Voltage signal from a droplet colliding with an optical probe

Normally, as shown in Fig. 4, the signal from the probe that is exposed to the air is constantly at  $V_G$ . Once a droplet collides with the probe tip (point A in Fig. 4), the signal drops instantly to  $V_L$  because the tip is surrounded by water. The signal stays at  $V_L$  until the droplet starts becoming isolated from the probe tip (point B). When the droplet is about to leave, the probe signal starts to rise linearly from  $V_L$  to  $V_G$ . The total time the droplet spends on the probe tip, from point A to point B in Fig. 4, is defined as the liquid presenting time ( $T_L$ ) while the time taken for the signal to rise from  $V_L$  to  $V_G$  is defined as the liquid de-wetting time ( $T_R$ ). However, according to Hong et al., (2004),  $T_R$  can be suitably evaluated between point C (which represents 10% of the difference between  $V_G$  and  $V_L$ ) and point D (which represents 70% of this difference) as the signal rise is linear and stable between these points. The  $T_L$  and  $T_R$  measured for each droplet could be used to compile its size and velocity.

### 2.3.2 Data interpretation

According to Hong et al., (2004), droplet velocity is proportional to its de-wetting time ( $T_R$ ). The relation between  $T_R$  and  $V_d$  is described in Equation (2) where  $L_s$  and  $b$  are the equation constants. These constants depend on the characteristics of each probe, which can be determined experimentally. In this experiment,  $L_s$  and  $b$  for the probe were equal to 17  $\mu\text{m}$  and -1, respectively.

$$V_d = L_s \cdot T_R^{-b} \quad (2)$$

Droplet size is calculated by multiplying the liquid presenting time ( $T_L$ ) and the droplet's velocity ( $V_d$ ) as expressed in Equation (3); where  $L_C$  is the chord length of a droplet that collides with the probe. Note that the size determined with this algorithm is the droplet chord length, not the droplet diameter.

$$L_C = V_d \cdot T_L \quad (3)$$

In the first part of the work, the syringe was set up above the very center of the optical probe. Therefore, a chord determined in the first part could be assumed to be the same as the droplet diameter. However, the experiment in the second part, using the industrial nozzle, was different since the position of contacting droplets could not be controlled. Consequently, in order to improve the algorithm accuracy, statistical and probability procedures for conversion of chord length distribution to diameter distribution

were applied for the spraying system. Various methodologies have been developed for this conversion (Cartellier, 1999). In this work, (Clark and Turton, 1988) methodology was selected to normalize the data since it is one of the reliable methods concerning the issue.

### 2.3.3 Probe limit

#### 2.3.3.1 Velocity limitation

In order to determine the limit of velocity measurement with the optical probe, its methodology needs to be recalled. The velocity of the droplet is calculated using the droplet dewetting time ( $T_r$ ) and applying it to Equation (2). Normally, the constant  $b$  in the equation is -1, so Equation (4) can be expressed as;

$$V_d = \left( \frac{L_s}{T_r} \right) \quad (4)$$

Since  $L_s$  is the constant parameter of the probe, the maximum velocity would occur when  $T_r$  is at its minimum value. The minimum value of  $T_r$  depends on the acquisition rate of the probe as well as the number of minimum points that can possibly be recorded on the experimental curve, as shown in Equation (5).

$$T_{R,min} = \left( \frac{\text{Acquisition rate}}{\text{No. of minimum points}} \right) \quad (5)$$

By combining with Equation (4), the maximum velocity that could be determined by the probe becomes;

$$V_{d,Max} = \left( \frac{L_s}{T_{R,min}} \right) = \left( \frac{L_s \times \text{Acquisition rate}}{\text{No. of minimum points}} \right) \quad (6)$$

From Equation (6), it indicates that the maximum velocity that the probe can theoretically detect depends on the probe characteristic constant ( $L_s$ ) and the acquisition rate of the probe.

#### 2.3.3.2 Size limits

The size limits of the optical probe could be determined in the same way as the velocity limits. The size of the droplet determined by the optical probe corresponds to Equation (3), is the product of the liquid presenting time ( $T_L$ ) by its velocity. Therefore, the minimum size limit would be acquired when the minimum  $T_L$  is considered. The minimum  $T_L$  is determined using the same approach as for the minimum  $T_R$  from Equation (5), i.e.

$$T_{L,min} = \left( \frac{\text{Acquisition rate}}{\text{No. of minimum points}} \right) \quad (7)$$

By combining with Equation (3), the minimum size that could be determined by the optical probe can be expressed as in Equation (8).

$$L_{c,min} = V_d \times T_{L,min} = V_d \times \left( \frac{L_s \times \text{Acquisition rate}}{\text{No. of minimum points}} \right) \quad (8)$$

From this equation, the minimum size ( $L_{c,min}$ ) is a function of the droplet's velocity ( $V_d$ ), the acquisition rate, the probe constant value, and the number of minimum points of  $T_L$ . When considering the maximum velocity for a certain acquisition rate and minimum number of points, Equation (8) becomes;

$$L_{c,min} @ V_{d,max} = \left( \frac{\text{No. of minimum points}}{\text{Acquisition rate}} \right) \times \left( \frac{L_s \times \text{Acquisition rate}}{\text{No. of minimum points}} \right) = L_s \quad (9)$$

When the same number of minimum points is considered for both  $T_L$  and  $T_R$ , the minimum sizes are equal to the probe constant ( $L_s$ ), regardless of the acquisition rates. However, it should be noted that the maximum velocity is different for different acquisition rates, which leads to a significantly different size limits at a certain velocity. Moreover, when the velocity of the measured droplet is lower than the maximum velocity, the size limit decreases following Equation (9).

### 2.3.3.3 Adjacent droplets filter

In this experiment, the concept to determine the droplet frequency limit that approaches a probe is developed based on the interval distance between each droplet. The pre-experiment indicated that there was a discrepancy between the probe and the high-speed camera when the number of droplets approaching the probe was high. This discrepancy occurred because the droplets are too close to each other; therefore, the chance of the droplet coalescence on the probe increased, leading to the large discrepancy between the two techniques.

In order to obtain the droplet frequency limit theoretically, the assumption of the droplets was set up as follow: (1) the droplet sizes and velocities of each droplet are the same (2) the interval distance between each droplet is equal and at least equal to their own diameter,  $d$ , to avoid the coalescence of each droplet. The conceptual diagram is as shown in Fig. 5.

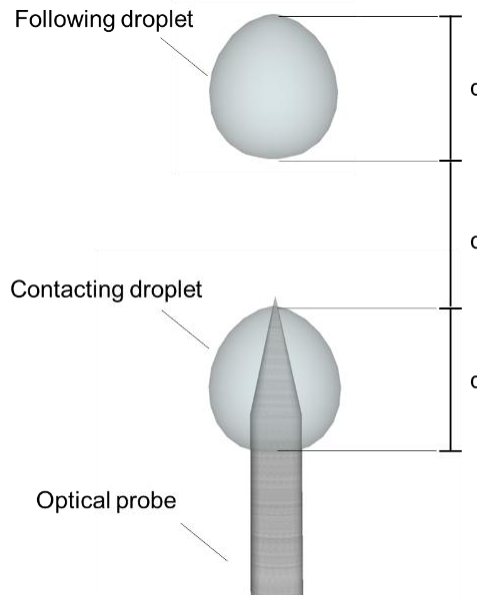


**Fig. 5** Minimum interval distance between each droplet for avoiding droplet coalescence

From the above concept, the time until the following droplet has to spend in order to collide with the probe ( $T_i$ ) is:

$$T_i = \frac{\text{distance}}{\text{velocity}} = \frac{d}{V_d} \quad (10)$$

and the time each droplet spends from contacting until leaving the probe or so-called the liquid presenting time ( $T_L$ ) is:

$$T_L = \frac{\text{distance}}{\text{velocity}} = \frac{d}{V_d} \quad (11)$$

Therefore, the total time of each droplet until the same cycle is repeated is the summation of  $T_i$  and  $T_L$  and the droplet frequency can be calculated from Equation (12)

$$f_L = \frac{1}{T_i + T_L} = \frac{V_d}{2d} \quad (12)$$

**Table 1** Droplet frequency limit for approaching the probe at various droplet velocities and sizes

Velocity (m/s)	Droplet frequency limit (Hz)										
	Droplet diameter (mm)										
	0.5	1.0	2.0	3.0	4.0	5.0	6.0	7.0	8.0	9.0	10
0.5	500	250	125	83	63	50	42	36	31	28	25
1.0	1,000	500	250	167	125	100	83	71	63	56	50
1.5	1,500	750	375	250	188	150	125	107	94	83	75
2.0	2,000	1,000	500	333	250	200	167	143	125	111	100
2.5	2,500	1,250	625	417	313	250	208	179	156	139	125
3.0	3,000	1,500	750	500	375	300	250	214	188	167	150
4.0	4,000	2,000	1,000	667	500	400	333	286	250	222	200
5.0	5,000	2,500	1,250	833	625	500	417	357	313	278	250
6.0	6,000	3,000	1,500	1,000	750	600	500	429	375	333	300
7.0	7,000	3,500	1,750	1,167	875	700	583	500	438	389	350
8.0	8,000	4,000	2,000	1,333	1,000	800	667	571	500	444	400
9.0	9,000	4,500	2,250	1,500	1,125	900	750	643	563	500	450
10.0	10,000	5,000	2,500	1,667	1,250	1,000	833	714	625	556	500

Table 1 shows the droplet frequency limit of each size and velocity of the droplets. The higher frequency beyond this table would have a large possibility to induce the droplet coalescence that leads to a discrepancy. In addition, with this assumption, the probe limit can be easily determined using the value of the local liquid fraction obtained in the experiment. When the local liquid fraction is higher than 50%, the limit according to Table 1 is achieved, thus the chance of the droplet coalescence on the probe increases and the discrepancy of the probe becomes larger. On the other hand, the accurate droplet velocity and size could be obtained when the local liquid fraction is below 50%. Note that the calculation of the local liquid fraction could be performed according to Equation (13) where the liquid fraction ( $\varepsilon_L$ ) can be simply calculated by summing all the droplet presenting times ( $T_L$ ) and dividing by the total time of acquisition.

$$\varepsilon_L = \left( \frac{\sum T_L}{\text{Total time of acquisition}} \right) \quad (13)$$

#### 2.4 Performance estimator

In order to compare and discuss the results from the high-speed camera and the optical probe equitably, the statistical parameter and methodologies were applied based on the comparing data of droplet velocities and their sizes.

For the comparison of the series of droplets produced by the syringe, the average absolute relative deviation (AARD) was used to determine the average deviation of every droplet velocity and size observed from different methods. AARD can be calculated from Equation (14) and Equation (15) for the velocity and size, respectively, where  $V_i$ ,  $d_i$  and  $N$  refer to the velocity obtained by each technique, the droplet size obtained by each technique, and the number of droplets used in the experiment. The subscription of HSC represents for the high-speed camera and OFP for the optical fiber probe.

$$\text{AARD of velocity} = \frac{1}{N} \left( \sum_i^N \left| \frac{V_{OFP} - V_{HSC}}{V_{HSC}} \right| \right) \times 100 \% \quad (14)$$

$$\text{AARD of size} = \frac{1}{N} \left( \sum_i^N \left| \frac{d_{OFP} - d_{HSC}}{d_{HSC}} \right| \right) \times 100 \% \quad (15)$$

For comparing the average velocities and sizes obtained from both techniques, the t-test, one of the most widely used hypothesis tests for the small number of samples, was applied (Montgomery and Runger, 2010). The Welch's t-test was used due to the different variances of each droplet velocity and size from each technique. The equations for the t-test are expressed in Equation (16) and Equation (17), where  $t_0$  is the t-score while  $\bar{X}_i$  and  $S_i^2$  are mean and variance of the sample from each technique, respectively.

$$t_0 = \frac{\bar{X}_{OFP} - \bar{X}_{HSC}}{S_t} \quad (16)$$

$$S_t = \sqrt{\frac{S_{OFP}^2}{n} + \frac{S_{HSC}^2}{n}} \quad (17)$$

To perform the hypothesis test, the p-value was used with the t-test. The p-value can be calculated from the probability of the sample that lies outside the range between  $-|t_0|$  and  $+|t_0|$  from its mean, which refers to the probability of the sample which deviated from its mean larger than  $t_0$ . When comparing the p-value with the significance level ( $\alpha$ ), which is the boundary level that statistically determines the statistical difference; if the p-value is larger than  $\alpha$ , the means of the samples are not statistically significantly different. In contrast, when the p-value is smaller than  $\alpha$ , it is remarked as a statistically significant different. Note that the exact value of the  $\alpha$  is not identified and typically set between 0.01 to 0.05, where the value of 0.05 is normally used.

For the spray case using the industrial nozzle, the Cohen's effect size method was used due to the very large number of droplets observed. As mentioned above, many thousand droplets were detected by both techniques where the comparison using Z-test or T-test would lead to a false determination (Sullivan and Feinn, 2012). Therefore, the Cohen's effect size method is suitable for this comparison, where the effect size ( $d_c$ ) can be determined using Equation (18).

$$d_c = \frac{\bar{X}_1 - \bar{X}_2}{S_t} \quad (18)$$

In the equation,  $\bar{X}_i$  is the mean of data group  $i$  and  $S_i$  is the standard deviation of either group. When the effect size is 0.2 or below, the deviation can be considered as small

where only 15 % of data was not overlap. While 0.5, 0.8, and 1.3 are considered as the medium, large, and very large deviations with the non-overlap percentage of 33, 47, and 66 %, respectively.

### 3. Results and Discussion

#### 3.1 Acquisition of the droplet series

##### 3.1.1 Droplet velocity

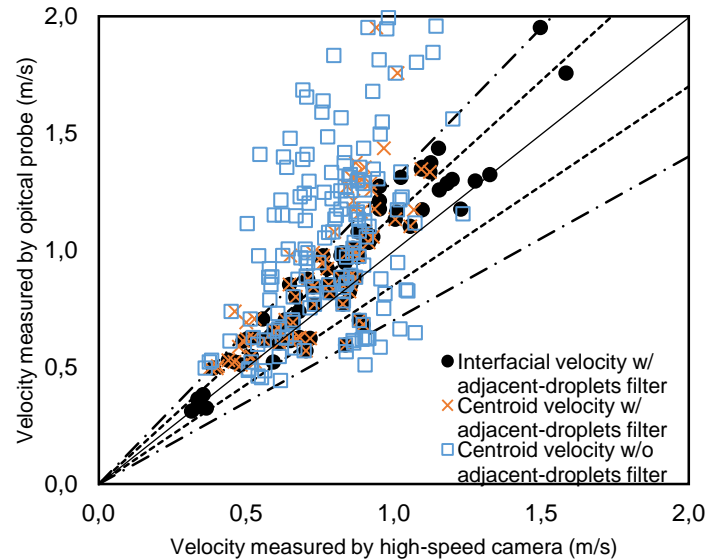


**Fig. 6** Velocities of the same droplets obtained with different methods

The droplet velocities obtained from both high-speed camera and optical probe data are illustrated in Fig. 6. A point in the figure represents a droplet velocity for the same droplet; the x-axis and y-axis are the droplet velocity determined with the high-speed camera and the optical probe, respectively. Each point of from the optical probe was compared with two different post processing methods: centroid and interfacial velocities. The adjacent-droplets filter was also applied in the of centroid velocity to eliminate droplets that were too close to each other which is the cause of the droplet coalescence. From the figure, it can be seen that the droplet velocities determined by the optical probe were in a good agreement with the interfacial velocity with adjacent-droplets filter one. The discrepancy was the smallest when comparing with the centroid velocity with filter and unfiltered centroid velocity, respectively. The droplet oscillation and droplet coalescence were responsible for the deviation.

The droplet coalescence occurred when two or more droplets arrived at the probe at almost the same time. As shown in Fig. 7, the coalescence between droplets gave a larger droplet; the droplet arriving slightly later would undergo a change in velocity due to the surface tension of water, which dragged it down rapidly.

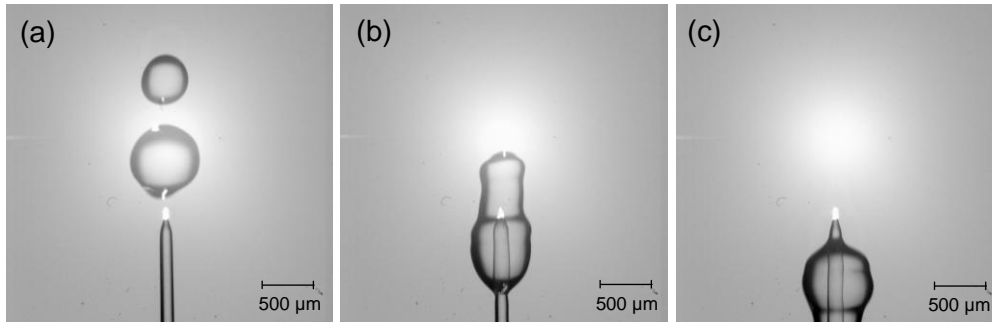


**Fig. 7** Droplet coalescence at the probe tip

(a) Droplets before collision (b) Coalescence on collision (c) Combined droplet after collision

Fig. 8 represents the interfacial velocity of the coalesced droplets at the probe tip as a function of distance from the probe. It can be seen that, at distances of more than 0.5 mm, the droplet moved at a velocity of around 1 m/s on average. However, at the instant of contact, the arriving droplet coalesced with the other droplet as shown in Fig. 7, and was dragged down by it, which increased its velocity dramatically.

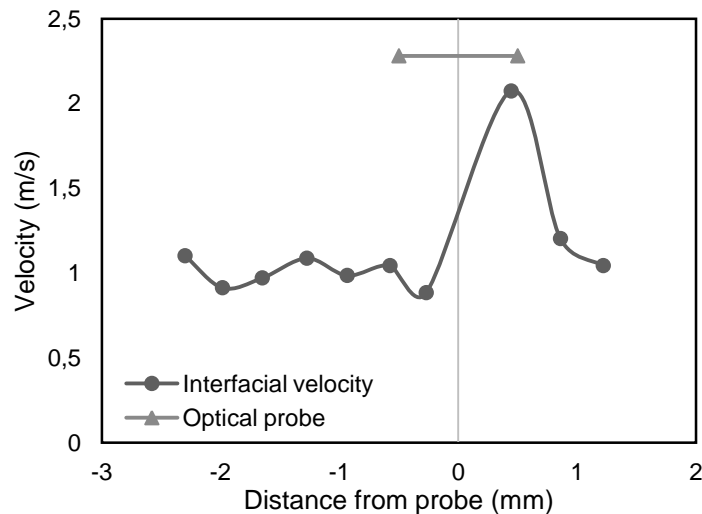


**Fig.8** Effect of droplet coalescence on the droplet interfacial velocity as a function of distance from the probe

In order to avoid the discrepancy due to the droplet coalescence, the adjacent-droplets filter on the data obtained by the optical probe is introduced. The principle of the filter is based on the droplet frequency which is the number of droplets observed by the probe per second, where the detail is mentioned previously in Section 2.3.3.3. The screening out eliminated the droplets that tend to cause the coalescence regime. In this experiment, the droplet frequency was in the range between 100 to 2500 droplets/second. According to Table 1, since the majority of velocities and sizes of droplets were around 1 m/s and 0.5 mm, respectively, the droplets having higher than 1,000 Hz was screened out. After applying the filter, as shown in Fig. 6, the centroid velocity with the adjacent-droplets filter shows a better result as compared with the unfiltered one. The droplets screened out were mostly the droplets having too high droplet frequency approaching the probe. However, with the filter, the droplet oscillation could not be eliminated and therefore the discrepancy still existed. From this point, it is obvious that one of the limits of the optical probe was the droplet frequency approaching the probe. The droplet coalescence tends to occur when too high droplet frequency or too dense spray occurred. In order to avoid this regime, the data filter

has to be applied or the optical probe should be used only in suitable conditions. Section 2.3.3.3 describes the limit of the optical probe and the appropriate range that the optical probe can perform accurately.

In addition, according to the probe methodology to determine droplet velocity, the probe examines the droplet velocity at the interface of the droplet when it is leaving the probe (Hong et al., 2004). Therefore, because of the oscillation of droplets that occurred since their formation process, when they came into contact with the optical probe as shown in Fig. 9, the droplet velocities could be recorded as faster or slower than the droplet centroid velocity, depending on the oscillating regime occurring at the time it was leaving the probe. Fig. 10 shows the droplet interfacial velocity determined by the high-speed camera versus its position before the droplets contact the optical probe tip.

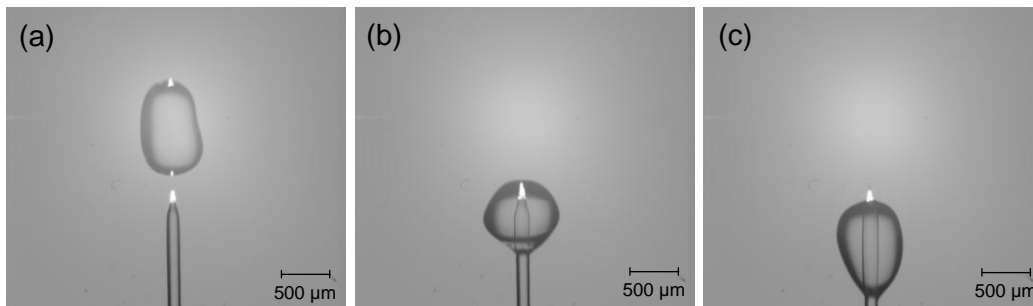


**Fig. 9** Droplet oscillation at the optical probe tip

(a) Stretching before collision (b) Shrinking during collision (c) Re-stretching after collision

As seen in Fig. 10, the interfacial velocity of the droplets varied around its centroid velocity (dashed line) due to the oscillation effect which occurred from the droplet formation. Therefore, the velocities of the droplets determined by the optical probe were dependent on their oscillating regime when they were leaving the probe. For droplets that were expanding, the velocities obtained from the probe would be smaller than the average velocity as shown in Fig. 10(a). On the other hand, the shrinking regime droplets would show faster velocities than their average, Fig. 10(b). This finding supports the experiment of Valero and Bung (2017) regarding their non-linear calibrations for high-velocity estimations with monofiber probes on multiphase flows (Valero and Bung, 2017).

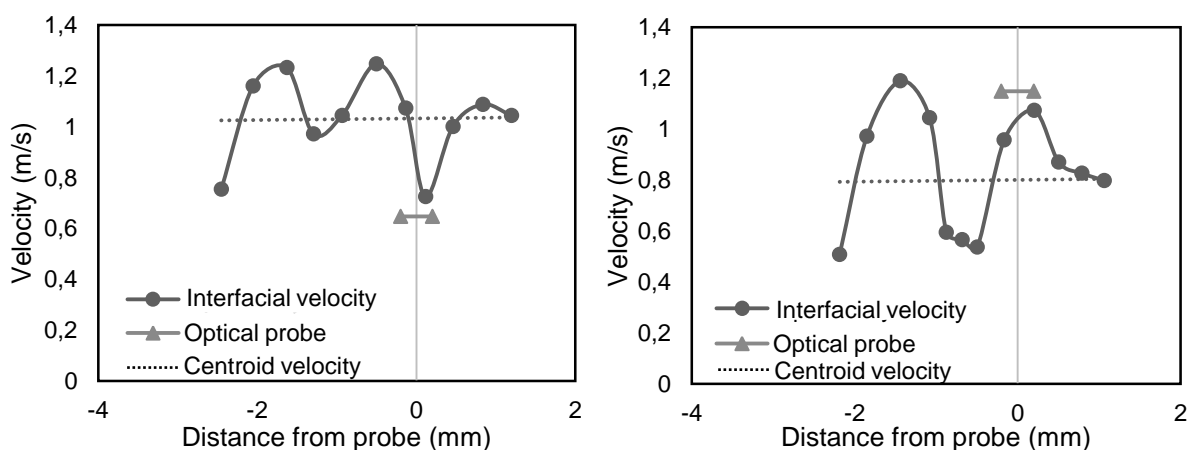
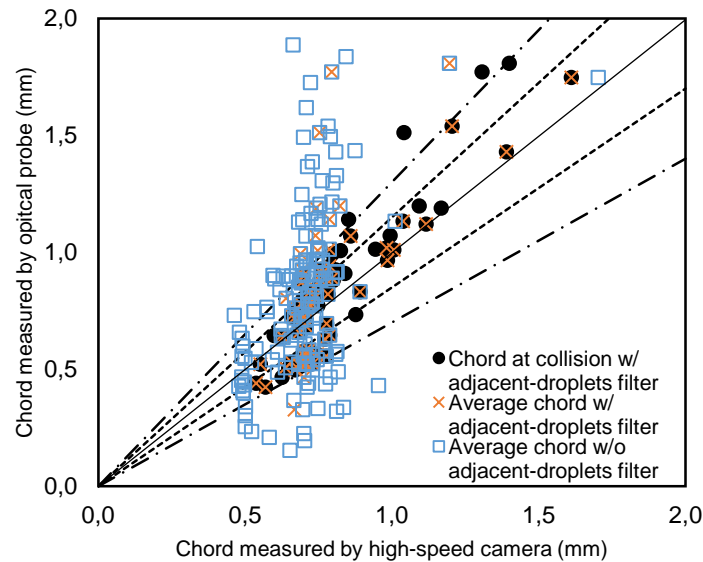


**Fig. 10** Effect of droplet oscillation on the droplet interfacial velocity according to the distance from the probe at a water injection rate of 0.128 mL/s (a) Expanding oscillation (b) Shrinking oscillation

In summary, due to the fact that the optical probe acquired the velocity at the droplet interface. Therefore, the suitable post-processing determination method for the high-speed camera was the interfacial velocity especially when the droplet oscillation was occurring within the observation area. Moreover, the adjacent-droplets filter should also apply for the determination since the droplet coalescence on the probe also caused the probe to overestimate the droplet velocities. This incident indicated that the probe has its own limit on the dense regime of the spray and therefore the data filter based on the droplet frequency should be performed.

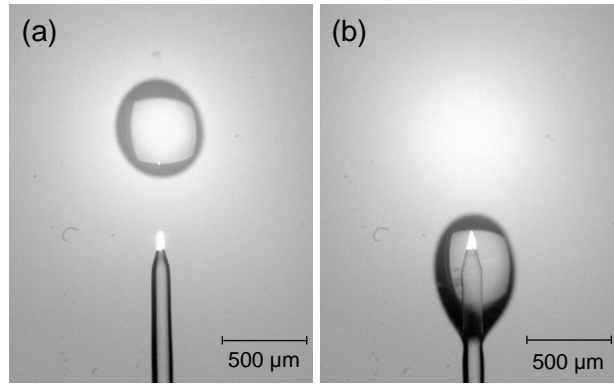
### 3.1.2 Droplet size

Fig. 11 shows the sizes in terms of chord for the same droplets determined with the high-speed camera (x-axis) and the optical probe (y-axis) for each post-processing method for the high-speed camera: average chord and the chord at the time of collision. The adjacent-droplets filter was also applied in order to observe the difference of the size after screening out the high acquisition frequency droplets.



**Fig. 11** Droplet chords of the same droplets obtained with different methods after applying frequency filter

It can be seen from the figure that the diameters determined by the optical probe showed a remarkable difference between when using the average chord from the high-speed camera especially when the adjacent droplets were not screened out. One of the major deviation was caused by the droplet coalescence as also shown in Fig. 7 when two adjacent droplets were collision at the probe at almost the same time and the droplet coalescence occurred at the probe tip leading to the formation of a large droplet that misled the optical probe signal. Hence, from Fig. 11, it can be seen that when the adjacent-droplets filter was applied, the chords determined by the high-speed camera were closer to those determined by the optical probe. In addition, the droplet oscillation was also one of the cause that contributed to the deviation because the optical probe determine the droplet size at the probe tip which was different from the average chord determination method of the high-speed camera, where both expanding and shrinking could lead to an overestimation or underestimation of the size. Therefore, it can be clearly seen that the results from the optical probe and the high-speed camera had a good agreement when the sizes of the droplets were determined at the collision period for the high-speed camera.



**Fig. 12** Droplet deformation  
(a) Before collision (b) After collision

In addition, the droplet deformation as shown in Fig. 12 also influenced the determination of size as it changed its shape after making contact with the probe because of the adhesive force (intermolecular force) between the droplet and the optical probe. Fig. 13 plots the droplet stream-wise diameter as a function of its distance from the probe. Before collision with the probe, the droplet diameter fluctuated around 0.65 mm. However, once the droplet collided with the probe, its diameter increased intensely due to the adhesive force. Consequently, the liquid presenting time was increased and the chord was overestimated.

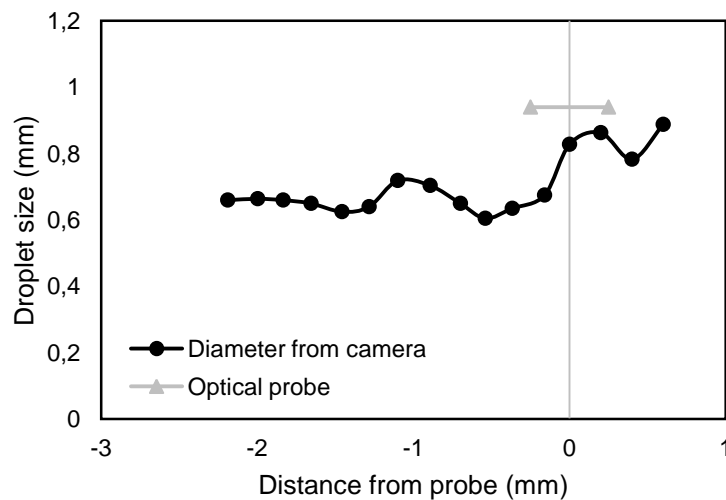


**Fig. 13** Effect of droplet deformation on the droplet diameter as a function of distance from the probe

In order to summarize statistically, Table 2 shows the average diameter and average velocity of all the droplets measured with different methods.

To include

1. Average velocity has less error with filter
2. Velocity of the optical probe were close to the interfacial velocity than the centroid velocity
3. Can be observed from higher P-value and lower AARD

It can be seen that the optical probe reported the average velocity slightly larger than that of the high-speed camera, while the average diameters were fairly close.

The AARD of the average velocity and diameter were at 35.44 and 32.42, respectively, where can be considered as a high deviation. Furthermore, the t-test used to indicate the difference between the average values of both technique indicated that the p-value of the average velocity and diameter were at 0.0002 and 0.3000, respectively, which referred to a highly significant difference in the case of the average velocity comparison.

**Table 2** Average diameter, velocity, and statistic estimator for the droplets obtained using the syringe for different methods

Image processing method		Adjacent droplets filter	Average				AARD (%)		P-value	
Velocity	Size		Velocity (m/s)		Size (mm)		Velocity	Size	Velocity	Size
			HSC	OPF	HSC	OPF				
Centroid	Average	No	0.78	1.04	0.72	0.83	40.31	34.54	0.000	0.003
			± 0.17	± 0.37	± 0.21	± 0.43				
Centroid	Average	Yes	0.76	0.91	0.89	0.99	21.29	22.29	0.000	0.251
			± 0.18	± 0.31	± 0.44	± 0.65				
Interfacial velocity	At collision	Yes	0.84	0.93	0.85	0.89	13.17	15.60	0.054	0.537
			± 0.24	± 0.31	± 0.30	± 0.45				

Size disutribution discusses in the same direction as the velocity

~~However, when the high acquisition frequency was screened out, the average velocity obtained from the probe reduced and became closer to the one obtained from the high-speed camera. The AARD of both average velocity and diameter were slightly smaller compared to the without screen out process. The p-values obtained from the test were 0.0372 and 0.5324 for the average velocity and size, respectively, indicating that the average velocity and size between both techniques were closer than without using the screen out process. At this point, the results statistically showed a better agreement since the p-value is 0.0372 which lies between the  $\alpha$  of 0.01-0.05 that normally used as a significant level of the t-test. It also presented that when the comparison was made statistically, especially after using the screen out process, the deviation did not seem to be extremely high as when comparing one by one which represented by the AARD.~~

It should be noted that the droplet velocity obtained from the syringe was lower than that in the actual spray system. When operating with the spray system, the oscillation velocity would be significantly different from the droplet moving velocity and the effect of the oscillation might be diminished. Moreover, the droplet coalescence on the probe would be reduced since the droplet frequency of the spray was lower, averagely 353.3 droplets per second when using the syringe and 35.6 droplets per second when using the spray. This incident occurred because the position of the probe according to the syringe was very smaller (5 mm) comparing to the spray (5 cm); Hence, most of the droplets injected by the syringe collided with the probe whereas only some droplets contacted with the probe in the spray case leading to smaller amounts and lower droplet frequency approaching the probe. Therefore, in order to understand the potential of the optical probe better, an experiment performed to determine the droplet size and velocity in a spray system is reported in the next section.

In summary, the droplet size and velocity determined from both techniques showed a discrepancy when comparing the same droplets. The major discrepancy was caused by the different approaches of the two techniques. Therefore, when involved with the droplet oscillation, both methods gave velocities and sizes of the oscillating droplets differently. In addition, the droplet deformation and the droplet coalescence on the probe were observed causing a deviation between the techniques.

### 3.2 Acquisition of a spray condition

The experimental setup in this part was the one described in subsection 2.1.2. Velocity and size distributions obtained with the optical probe and the high-speed camera were compared. Note that, in this experiment, droplets were not necessarily pierced by the probe along their diameter; they were pierced at random positions. Therefore, the size measured by the optical probe was often along a chord, not a diameter. The data post-processing proposed by Clark and Turton, (1988) was therefore applied so that the sizes could be compared.

#### 3.2.1 Velocity distribution

Fig. 14 shows the velocity distributions observed by the high-speed camera and by the optical probe at a liquid flow rate of 0.59 LPM. In the figure, the droplet velocities characterized by both pieces of equipment show the same trends, with the average velocity of 7.20 and 7.13 m/s for the high-speed camera and the optical probe, respectively. The negative skewness was obtained by the high-speed camera while the nearly normal distribution was observed from the optical probe. Table 3 shows the average velocity of each technique along with its statistical values. According to Cohen's effect size, the effect size between both methods was 0.10 which corresponds to the non-overlapping percent of 7.8% that considered as a small deviation. Note that the large deviation found in the previous section did not occur here and it is apparent that the effects of droplet oscillation and coalescence became less significant when the probe was used in the real-world spray system where the droplets are smaller, moving faster, and less dense, where the average droplet frequency of droplets produced by the syringe was 353.3 droplets per second comparing to 35.6 droplets per second when used the industrial nozzle.

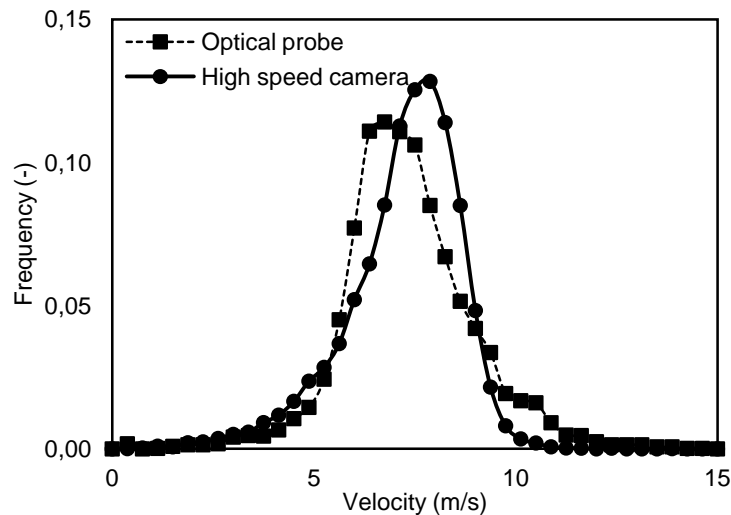


**Fig. 14** Velocity distribution of a spray system with the 0.89 mm nozzle size when operating at 0.59 L/min

In addition, firstly, the lowest droplet diameter limit of the high-speed camera was approximately 0.1 mm, while the optical probe was capable to detect droplets with a smaller diameter. The velocities of larger droplets are normally higher than those of smaller droplets, so the velocity distribution measured by the high-speed camera would shift toward the slightly higher values and appear in the negative skewness shape as shown in the result. Secondly, the optical probe did not always pierce the droplets along their center line, which led to underestimated measurements of the velocities. This phenomenon was originally reported by Hong et al., (2004). According to these explanations, the distribution of the

velocity observed by the high-speed camera was apparently at a higher velocity than that of the optical probe.

### 3.2.2 Size distribution

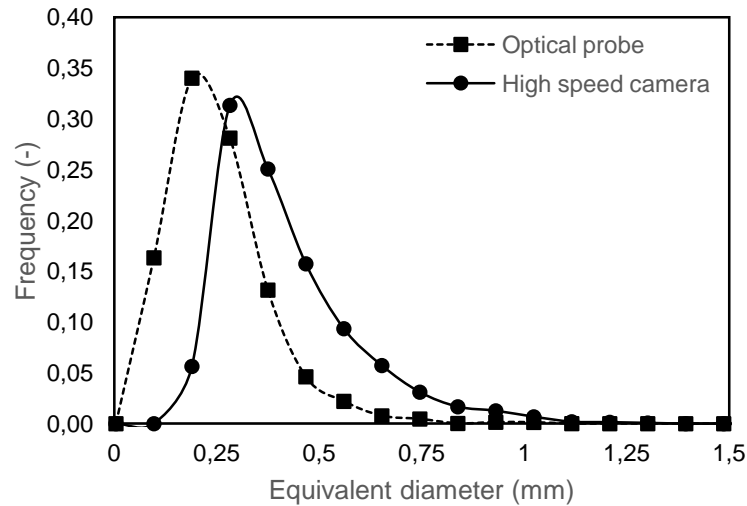


**Fig. 16** Size distribution of a spray system with the 0.89 mm nozzle size when operating at 0.59 L/min

The size distributions determined by both types of equipment are shown in Fig. 16. The droplet sizes determined by the optical probe were significantly smaller than those given by the high-speed camera. The Cohen's effect size as shown in Table 3 from both techniques gave the value of 1.03 where the large difference was indicated. Three effects were presumed to be the causes of this deviation. Firstly, the size limit difference between the two types of equipment might significantly affect this result. As mentioned earlier, the size limit of the high-speed camera used in this experiment was 0.1 mm, while that of the optical probe was significantly lower. The size limit of the probe will be analyzed and discussed in the next section. Secondly, the underestimated value of velocity mentioned earlier might have lowered the chord lengths determined by the probe since the chords detected by the probe were calculated from the droplet velocities. The third effect can be assumed to be due to the processing of the optical probe data when the probe was used with the spraying system. Unlike those produced by the syringe, droplets generated by the industrial nozzle contacted the probe randomly, and often not in the center of the probe. Consequently, the result obtained by the optical probe was the chord distribution rather than the diameter distribution. Thus, probabilistic data processing needed to be performed. Accordingly, the results from the data treatment were not direct measurements and could lead to the deviation. However, it should be noted that the deviation was not due to the probe providing false measurements since the results from the section comparing identical droplets were satisfactory.

**Table 3** Average diameter, velocity, and statistic estimator for the droplets obtained using the spray

Variable	High-speed camera	Optical probe	Cohen's Effect size	Estimated Percent of non-overlap
----------	-------------------	---------------	---------------------	----------------------------------

Average velocity (m/s)	7.20 ± 1.42	7.13 ± 1.60	0.10	7.8 %
Average diameter (mm)	0.251 ± 0.168	0.208 ± 0.139	1.03	57 %

### 3.3 Probe potential and limitations

#### 3.3.1 Velocity limitation

**Table 4** Velocity and size limits of the optical probe

Acquisition Rate (MHz)	Max velocity (m/s)				Min chord (μm)				
	3 points	5 points	7 points	10 points	V <sub>max</sub>	0.8V <sub>max</sub>	0.5V <sub>max</sub>	0.3V <sub>max</sub>	0.1V <sub>max</sub>
1	5.7	3.4	2.4	1.7	17.0	13.6	8.5	5.1	1.7
2	11.3	6.8	4.9	3.4	17.0	13.6	8.5	5.1	1.7
3	17.0	10.2	7.3	5.1	17.0	13.6	8.5	5.1	1.7
4	22.7	13.6	9.7	6.8	17.0	13.6	8.5	5.1	1.7
5	28.3	17.0	12.1	8.5	17.0	13.6	8.5	5.1	1.7
6	34.0	20.4	14.6	10.2	17.0	13.6	8.5	5.1	1.7

From Equation (6), it is clear that the maximum velocity limit depends on three variables: the probe constant ( $L_s$ ), the number of minimum points possibly recorded on the experimental curve, and the acquisition rate. By using the  $L_s$  of the probe and varying its acquisition rate, the maximum velocity limit can be expressed as shown in Table 4 as a function of the number of minimum points. The number of minimum points usually ranges between 3 and 10 and the acquisition rate was varied from 1 to 6 MHz.

In the table, increasing the acquisition rate raises the maximum velocity limit for each number of minimum points. The difference of the number of minimum points also changes the maximum velocity: the more numerous the points used for  $T_r$ , the lower the limit for the maximum velocity that can be observed by the probe. With higher numbers of points, higher signal accuracy is obtained. Therefore, in order to obtain the best result for the velocity determined by the optical probe, the highest possible acquisition rate is recommended. However, the amount of memory consumed by the acquisition system should also be considered.

Fig. 17 shows the effect of the acquisition rate on the droplet velocity determination by the optical probe and compares the results with that from the high-speed camera. The result from the high-speed camera indicates that the range of droplet velocities with the spray system was 5-12 m/s. The results from the optical probe for acquisition rates higher than 2 MHz show the same trends as the result from the high-speed camera. However, the result for 1 MHz acquisition rate has largely deviated. According to Table 4, the maximum velocity that can be determined with the 1 MHz acquisition rate is lower than 5.7 even for 3 minimum points. This result confirms the calculation used for the determination of the maximum velocity limit.

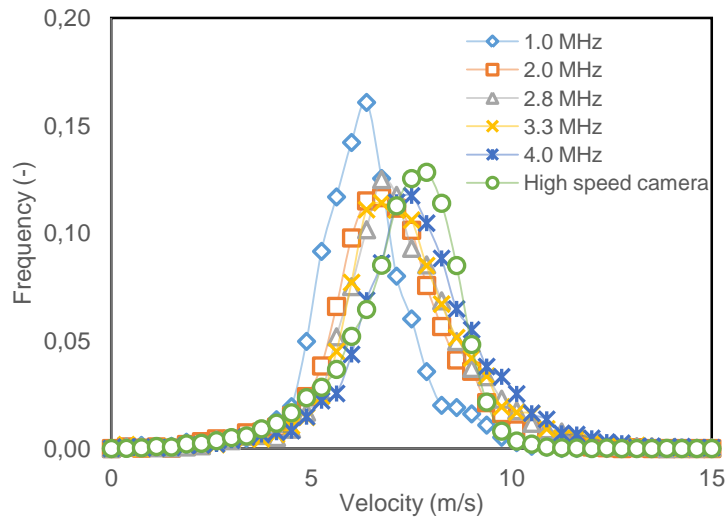


**Fig. 17** Effect of optical probe acquisition rate in a spray system with the 0.89 mm nozzle size operating at 0.59 L/min, and comparison with the high-speed camera results

### 3.3.2 Size limits

Table 4 indicates the minimum chord that can possibly be measured with the optical probe used in this experiment. It shows that, when operating at 10 % of the maximum velocity, the minimum size that the probe can determine is 1.7  $\mu\text{m}$ , which is very much smaller than with the high-speed camera. However, it should be noted that the size limit mentioned in Table 4 was calculated theoretically. In the actual regime, the very small droplets may have been destroyed by collisions and, moreover, the probability of small droplets coming into contact with the probe is extremely small.

In summary, the minimum size limit of the optical probe mainly depends on the ratio between droplet velocity and the maximum velocity ( $V/V_{\text{max}}$ ). With the lowest ratio of  $V/V_{\text{max}}$ , the smallest size limit can be reached. Note that the maximum velocity is strongly dependent on the acquisition rate. Therefore, the use of a high acquisition rate not only yields high accuracy but also extends the limits of the optical probe.

### 3.3.3 Advantages and drawbacks

With the results shown in the previous section, it is clear that the optical probe has the potential to determine the hydrodynamics of spray systems. However, to reach its full potential, the optical probe should be used in the right conditions. Table 5 summarizes the advantages and disadvantages of optical probes and high-speed cameras.

**Table 5** Advantages and disadvantages of optical probe and high-speed camera for determination of droplet size and velocity

High-speed camera	Optical probe
<p><b>Advantages</b></p> <ul style="list-style-type: none"> <li>• Can be visualized</li> <li>• Determines droplet size and velocity directly</li> <li>• Plane measurement</li> </ul>	<p><b>Advantages</b></p> <ul style="list-style-type: none"> <li>• Able to detect very small droplet sizes</li> <li>• Liquid fraction determination</li> <li>• Can be used in mildly dense spray conditions</li> </ul>
<p><b>Disadvantages</b></p> <ul style="list-style-type: none"> <li>• Requires a camera with high</li> </ul>	<p><b>Disadvantages</b></p> <ul style="list-style-type: none"> <li>• Cannot measure droplet diameter</li> </ul>

- |   |   |
|---|---|
| <ul style="list-style-type: none"> <li>• resolution and high frame rate</li> <li>• Requires an accurate and effective image processing method</li> <li>• Can be used only for visible conditions i.e. not good with dense spraying</li> </ul> | <ul style="list-style-type: none"> <li>• directly</li> <li>• High deviation if used with small numbers of droplets</li> <li>• Measures interfacial velocities of droplets (Oscillation velocities are included)</li> <li>• Point measurement</li> <li>• Requires calibration</li> </ul> |
|---|---|
- 

One of the major advantages of the optical probe is that it can be used in mildly dense spraying conditions, which are difficult to capture and process accurately with high-speed cameras. However, it was found that the probe should not be used at highly dense spray conditions without screening process since the droplet coalescence would lead to a large discrepancy. Moreover, the probe can determine the local liquid fraction directly, which the high-speed camera is not able to do.

In addition, the optical probe size and velocity limits are superior to those of high-speed cameras. The camera requires a very high acquisition rate and also a high resolution in order to provide good accuracy. However, the optical probe also has the great disadvantage of not being able to measure droplet sizes directly and requires a probability-based method in order to obtain the predicted diameter distribution result. Moreover, the probe is also handicapped by the effect of droplet oscillation when determining low droplet velocities (less than 2 m/s) because of its methodology of measuring droplet velocities by their interfacial velocity. Fortunately, the effect of droplet oscillation and coalescence are less significant when operating with usual spraying systems. However, more information and further studies regarding the spray characterization for the current industrial sprays that use the optical probe are needed, for instance, the study of sprays comparing with a high-speed camera or PDA.

#### 4. Conclusion

The experiment was set up in the aim of identifying the potential of an optical probe when it is used to determine the hydrodynamics of spray systems. The accuracy of the probe was assessed by comparing its results with those from a high-speed camera.

When comparing the series of droplets produced by a syringe as the nozzle, it was found that the optical probe gave an explainable discrepancy comparing with that of the high-speed camera. The deviation was introduced by the different methodologies of the two techniques. The optical probe determined droplet velocities and sizes at the interface of droplets, while the high-speed camera determined them from the displacement of droplet centroids. Therefore, when observing oscillating droplets, the two techniques gave different results. Values could be overestimated or underestimated by the optical probe depending on the oscillating regime of droplets when contacting the probe. Droplet coalescence also influenced the probe results. However, the acquisition of frequency data treatment can be performed to eliminate the effect of droplet coalescence. It also found that the comparing velocity and size results between the optical probe and the high-speed camera were in good agreement especially when using average values rather than comparing one by one.

When operating in the industrial spray conditions, consistent results, especially for the velocity distributions, were achieved with the optical probe and the high-speed camera. The oscillation and coalescence effects were significantly diminished because the droplets in

the spray had smaller sizes, higher velocities, and less dense when compared to the droplets produced using the syringe. The deviation was generally presented, especially in the size of the droplets and it was logically presumed to arise from the off-center contact between the probe and the droplets, the post-processing methodology, and the size limits of the two techniques. In addition, the probe limits in the velocity and size measurement were calculated theoretically and the results showed that the velocity and size limits were strongly dependent on the acquisition rate. With a 4-MHz acquisition rate, the probe was theoretically able to detect a droplet that having the highest velocity of up to 22.7 m/s and the lowest size of approximately 17  $\mu\text{m}$ . The acquisition frequency limit was also theoretically determined, and it is noticeable that the frequency limit was depended on the velocity and size of the droplets.

In addition, one of the advantages of the optical probe is that it can directly measure the liquid fraction of the spray system and, moreover, able to determine droplet velocities and sizes in mildly dense spray conditions, which is hard to perform using a high-speed camera or other optical techniques. However, it should be noted that, when the local liquid fraction is larger than 50%, the discrepancy of the probe is highly induced by the droplet coalescence. Therefore, the accurate droplet velocity, as well as the size, could be obtained when the local liquid fraction is below 50%.

### Nomenclature

A	area ( $\text{mm}^2$ )
AARD	absolute average relative deviation (%)
b	probe exponential constant (-)
d	droplet diameter (mm)
$d_c$	Cohen's effect size
$d_e$	equivalent spherical diameter (mm)
$f_L$	theoretical acquisition frequency limit ( $\text{s}^{-1}$ )
$L_C$	chord length (mm)
$L_{c,\text{min}}$	minimum detectable chord ( $\mu\text{m}$ )
$L_s$	probe constant ( $\mu\text{m}$ )
N	Number of data (-)
P	perimeter (mm)
S	standard deviation
$S^2$	variance
$t_o$	t-score for hypothesis test
$T_i$	time interval between each droplet ( $\mu\text{s}$ )
$T_L$	liquid presenting time ( $\mu\text{s}$ )
$T_{L,\text{min}}$	minimum liquid presenting time ( $\mu\text{s}$ )
$T_r$	de-wetting time ( $\mu\text{s}$ )
$T_{R,\text{min}}$	minimum de-wetting time ( $\mu\text{s}$ )
$V_d$	droplet velocity ( $\text{m s}^{-1}$ )
$V_G$	gas level voltage (V)
$V_L$	liquid level voltage (V)
$V_{d,\text{max}}$	maximum detectable velocity (m/s)

### Greek Letters

$\varepsilon_L$	local liquid fraction (-)
$\alpha$	significance level of rejection a hypothesis

### Subscription

HSC high-speed camera  
OFP optical fiber probe

## Acknowledgments

The authors acknowledge the financial support given by the Research Program in Control of Hazardous Contaminants in Raw Water Resources for Water Scarcity Resilience, Center of Excellence on Hazardous Substance Management (HSM) and Research Unit on Technology for Oil Spill and Contamination Management, Chulalongkorn University, and precious technical support of Claude Le Men and José Moreau.

## References

- Abuaf, N., Jones, O.C., Zimmer, G.A., 1978. Optical probe for local void fraction and interface velocity measurements. *Rev. Sci. Instrum.* 49, 1090. <https://doi.org/10.1063/1.1135524>
- Bandyopadhyay, A., Biswas, M.N., 2007. Modeling of SO<sub>2</sub> scrubbing in spray towers. *Sci. Total Environ.* 383, 25–40. <https://doi.org/10.1016/j.scitotenv.2007.04.024>
- Bashipour, F., Khorasani, S.N., Rahimi, A., 2015. H<sub>2</sub>S Reactive Absorption from Off-Gas in a Spray Column: Insights from Experiments and Modeling. *Chem. Eng. Technol.* 38, 2137–2145. <https://doi.org/10.1002/ceat.201500233>
- Bung, D.B., Valero, D., 2016. Optical flow estimation in aerated flows. *J. Hydraul. Res.* 54, 575–580. <https://doi.org/10.1080/00221686.2016.1173600>
- Cartellier, A., 1999. Post-treatment for phase detection probes in non uniform two-phase flows. *Int. J. Multiph. Flow* 25, 201–228. [https://doi.org/10.1016/S0301-9322\(98\)00041-X](https://doi.org/10.1016/S0301-9322(98)00041-X)
- Cartellier, A., Achard, J.L., 1991. Local phase detection probes in fluid/fluid two-phase flows. *Rev. Sci. Instrum.* 62, 279–303. <https://doi.org/10.1063/1.1142117>
- Chigier, N., 1983. Drop size and velocity instrumentation. *Prog. Energy Combust. Sci.* 9, 155–177. [https://doi.org/10.1016/0360-1285\(83\)90008-4](https://doi.org/10.1016/0360-1285(83)90008-4)
- Clark, N.N., Turton, R., 1988. Chord length distributions related to bubble size distributions in multiphase flows. *Int. J. Multiph. Flow* 14, 413–424. [https://doi.org/10.1016/0301-9322\(88\)90019-5](https://doi.org/10.1016/0301-9322(88)90019-5)
- Darake, S., Hatamipour, M.S., Rahimi, A., Hamzeloui, P., 2016. SO<sub>2</sub> removal by seawater in a spray tower: Experimental study and mathematical modeling. *Chem. Eng. Res. Des.* 109, 180–189. <https://doi.org/10.1016/j.cherd.2015.11.027>
- Felder, S., Chanson, H., 2015. Phase-detection probe measurements in high-velocity free-surface flows including a discussion of key sampling parameters. *Exp. Therm. Fluid Sci.* 61, 66–78. <https://doi.org/10.1016/j.expthermflusci.2014.10.009>
- Felder, S., Pfister, M., 2017. Comparative analyses of phase-detective intrusive probes in high-velocity air–water flows. *Int. J. Multiph. Flow* 90, 88–101. <https://doi.org/10.1016/j.ijmultiphaseflow.2016.12.009>
- Hariz, R., del Rio Sanz, J.I., Mercier, C., Valentin, R., Dietrich, N., Mouloungui, Z., Hébrard, G., 2017. Absorption of toluene by vegetable oil–water emulsion in scrubbing tower: Experiments and modeling. *Chem. Eng. Sci.*, 12th International Conference on Gas-Liquid and Gas-Liquid-Solid Reactor Engineering 157, 264–271. <https://doi.org/10.1016/j.ces.2016.06.008>
- Heyt, J., Diaz, J., 1975. Pressure drop in flat-oval spiral air duct. *ASHRAE Trans.* 81, 221–230.
- Hong, M., Cartellier, A., Hopfinger, E.J., 2004. Characterization of phase detection optical probes for the measurement of the dispersed phase parameters in sprays. *Int. J. Multiph. Flow* 30, 615–648. <https://doi.org/10.1016/j.ijmultiphaseflow.2004.04.004>
- Husted, B.P., Petersson, P., Lund, I., Holmstedt, G., 2009. Comparison of PIV and PDA droplet velocity measurement techniques on two high-pressure water mist nozzles. *Fire Saf. J.* 44, 1030–1045. <https://doi.org/10.1016/j.firesaf.2009.07.003>

- Jones, D.P., Watkins, A.P., 2012. Droplet size and velocity distributions for spray modelling. *J. Comput. Phys.* 231, 676–692. <https://doi.org/10.1016/j.jcp.2011.09.030>
- Marty, S., Matas, J.-P., Cartellier, A., 2013. Study of a liquid–gas mixing layer: Shear instability and size of produced drops. *Comptes Rendus Mécanique, Combustion, spray and flow dynamics for aerospace propulsion* 341, 26–34. <https://doi.org/10.1016/j.crme.2012.10.009>
- Montgomery, D.C., Runger, G.C., 2010. *Applied Statistics and Probability for Engineers*. John Wiley & Sons.
- Neal, L.G., Bankoff, S.G., 1963. A high resolution resistivity probe for determination of local void properties in gas-liquid flow. *AIChE J.* 9, 490–494. <https://doi.org/10.1002/aic.690090415>
- Nicholas P. Cheremisinoff, 1986. *Encyclopedia of Fluid Mechanics: Gas-Liquid Flows, Encyclopedia of Fluid Mechanics*. Gulf Publ. Company.
- Raghunath, C.V., Mondal, M.K., 2016. Reactive absorption of NO and SO<sub>2</sub> into aqueous NaClO in a counter-current spray column. *Asia-Pac. J. Chem. Eng.* 11, 88–97. <https://doi.org/10.1002/apj.1946>
- Roustan, M., 2003. *Transferts gaz-liquide dans les procédés de traitement des eaux et des effluents gazeux*. Tec & Doc.
- Saito, T., 2017. Optical Fibre Probing for Bubble/Droplet Measurement, and Its Possibility of the Application to Biotechnology, in: *Recent Global Research and Education: Technological Challenges, Advances in Intelligent Systems and Computing*. Springer, Cham, pp. 231–246. [https://doi.org/10.1007/978-3-319-46490-9\\_33](https://doi.org/10.1007/978-3-319-46490-9_33)
- Stevenin, C., Tomas, S., Vallet, A., Amielh, M., Anselmet, F., 2016a. Flow characteristics of a large-size pressure-atomized spray using DTV. *Int. J. Multiph. Flow* 84, 264–278. <https://doi.org/10.1016/j.ijmultiphaseflow.2016.05.004>
- Stevenin, C., Vallet, A., Tomas, S., Amielh, M., Anselmet, F., 2016b. Eulerian atomization modeling of a pressure-atomized spray for sprinkler irrigation. *Int. J. Heat Fluid Flow* 57, 142–149. <https://doi.org/10.1016/j.ijheatfluidflow.2015.11.010>
- Sullivan, G.M., Feinn, R., 2012. Using Effect Size—or Why the P Value Is Not Enough. *J. Grad. Med. Educ.* 4, 279–282. <https://doi.org/10.4300/JGME-D-12-00156.1>
- Tamhankar, Y., King, B., Whiteley, J., Cai, T., McCarley, K., Resetarits, M., Aichele, C., 2015. Spray absorption of CO<sub>2</sub> into monoethanolamine: Mass transfer coefficients, droplet size, and planar surface area. *Chem. Eng. Res. Des.* 104, 376–389. <https://doi.org/10.1016/j.cherd.2015.08.012>
- Tatin, R., Moura, L., Dietrich, N., Baig, S., Hébrard, G., 2015. Physical Absorption Of Volatile Organic Compounds By Spraying Emulsion In A Spray Tower: Experiments And Modelling. *Chem. Eng. Res. Des.*
- Tuck, C.R., Ellis, M.C.B., Miller, P.C.H., 1997. Techniques for measurement of droplet size and velocity distributions in agricultural sprays. *Crop Prot.* 16, 619–628. [https://doi.org/10.1016/S0261-2194\(97\)00053-7](https://doi.org/10.1016/S0261-2194(97)00053-7)
- Valero, D., Bung, D.B., 2017. Artificial Neural Networks and pattern recognition for air-water flow velocity estimation using a single-tip optical fibre probe. *J. Hydro-Environ. Res.* <https://doi.org/10.1016/j.jher.2017.08.004>
- Zhang, G., Chanson, H., 2018. Application of local optical flow methods to high-velocity free-surface flows: Validation and application to stepped chutes. *Exp. Therm. Fluid Sci.* 90, 186–199. <https://doi.org/10.1016/j.expthermflusci.2017.09.010>